Beyond Log-Normal Distributions: Hermite Spectra for Solving Population Balances

Robert A. Hamilton, Jennifer S. Curtis, and Doraiswami Ramkrishna
School of Chemical Engineering, Purdue University, West Lafayette, IN 47907

The oft-used log-normal distribution for solving many population-balance problems is in fact a degenerate case of a Hermite function expansion of the solution in log particle-size coordinate. Corrective capabilities of such an expansion constitute vast improvements not only over those using the log-normal distribution, but also over discretization methods in that moments other than those designed for in the latter are predicted with much higher accuracy, although at greater computational cost. The Hermite spectral method is compared with known analytical results and other computational techniques for particle dynamic processes involving agglomeration, breakage, and growth. This method is extremely accurate and flexible, as evidenced by the wide range of problems it can solve, both transient and steady state, along with perfectly mixed or convection dominant problems. Particle distributions are allowed to evolve according to the physics of the process, not constrained by restrictive assumptions inherent in the prespecified form of the distribution.

Introduction

Dispersed particles are encountered in a wide variety of systems. Spray drying, atmospheric pollution and air-quality studies, deposition of drugs or toxins in the human respiratory tract, the grinding of grains of corn or wheat, and cell cultures in bioreactors are a few examples where a population balance is applicable. The particle phase varies not only over external coordinates, the familiar space and time, but also over internal coordinates, which allows one to describe particles by any other useful parameter. One of the more common and thoroughly studied internal coordinates is particle volume, the internal coordinate this work will exclusively consider.

A number density function is assumed to exist that describes the average number of particles at each point in external and internal space. Changes in the number density function, that is, the particle volume distribution, are accounted for by the population-balance equation. Details of the derivation of the population-balance equation can be found in Ramkrishna (2000).

Simulation of evolving volume distributions can be accomplished by means of many different tools, generally broken into two main categories: discrete and continuous representations of the particle-size distribution. Using discrete variables, the number of particles in bins varies in time, with the possibility of the bins themselves changing. These techniques can be computationally very efficient, but care must be taken so that the most important quantities are accurately predicted. Oftentimes, rapidly changing systems require minute bins, and similarly small discretizations of time in order to achieve accurate results. The two equation models of Kumar and Ramkrishna (1996a,b) allow for only two quantities to be conserved, for example, mass and numbers. Any other quantities, such as the second moment, will suffer inaccuracies.

If a continuous function is used to describe the distribution, the necessary information can be derived. Numbers, mass, the second moment, or any other quantity can all be calculated given an accurate functional representation—and then the moments' data can be used to derive any pertinent information. Optical properties of the particles, for instance, can be written in terms of the moments of the particle size distribution (Wright, 2000).

When the details of the process are known, an assumption can be made about the form of the volume distribution function. Log-normal distributions have been an oft-popular choice. This distribution is said to "frequently arise in naturally occurring processes" and with distributions of fine particles (Fan and Zhu, 1998). Based upon an implementation of the central limit theorem of statistics, log-normal distributions arise from the product of two or more normal distribu-

Correspondence concerning this article should be addressed to D. Ramkrishna.

tions (Devore, 1995), and have been used to describe agglomeration events for this reason (for example, see Montroll and Shlesinger, 1984). In addition to the theoretical, some measured particle distributions can be fit adequately by log-normal distributions. As a few examples, Rosen and Greegor (1974) matched the log-normal function to jet-soot emissions; the particles from an oil-fueled burner were found to be distributed log-normally by Markowski and coworkers (1984); Park and Lee (2000) describe the deposition of radioactive aerosols within liquid–metal fast breeder reactors via log-normal particle-size distributions; and Dunbar and Hickey (2000) fit data from various inhaled pharmaceutical particles to log-normal, modified gamma, and other functions.

For a similar reason, the (modified) gamma distribution is regularly used to approximate breakage processes. First, a gamma distribution results from a limit in a similarity solution for pure binary fragmentation processes (Peterson, 1986). Physically, the brittle fracturing of a particle can be viewed as a fractal process. Based upon the fractal assumption, the Weibull distribution results as a solution to the pure breakage problem (Brown and Wohletz, 1995). Gamma, exponential, Rosin-Rammler, and Weibull distributions are all members of a similar family, where by a change of constants, one distribution can often be written in terms of the others in this family. Of this family, gamma distributions have typically yielded the best fits to experimental data, such as raindrop distributions in clouds (Miles et al., 2000; Testud et al., 2001).

This work presents a method by which a continuous number-density function can be achieved without restricting it to one of the traditional functional forms, such as the log-normal or gamma distribution. An orthogonal series, also known as a Hermite spectral approximation, is used to construct the number density in this work, and the coefficient of each term in the series evolves according to the processes the particles undergo. Hermite polynomials specifically form a spectral series based upon the log-normal distribution, so that a one-term spectral approximation is identical to the log-normal approximation to a number-density function. The supplementary terms of the Hermite series are then higher-order corrections to the log-normal approximation.

Population Balance Equations and Their Methods of Solution

The average number of particles in the infinitesimal volume $dV_x dV_r$ (in particle state space dV_x of internal coordinates and dV_r of external coordinates) is $f_1(\boldsymbol{x},\boldsymbol{r},t)dV_x dV_r$, where f_1 is the average number density function (with the explicit dependence on internal coordinates, external coordinates, and time dropped in this and all future nomenclature). Population-balance equations describe the evolution of this number density function. For a distribution where particle volume, v, is the only internal variable, the population balance equation is (Ramkrishna, 2000)

$$\frac{\partial}{\partial t^*} f_1^* + \frac{\partial}{\partial v^*} \dot{V}^* f_1^* + \nabla_r^* \cdot \dot{\boldsymbol{R}}^* f_1^* - \nabla_r^* \cdot D^* \nabla_r^* f_1^* = h^*. \quad (1)$$

The terms on the lefthand side of Eq. 1 are the local rate of change, growth, convection, and diffusion terms, respectively ($\dot{V}$ is the growth rate, $\dot{\boldsymbol{R}}$ is the particle velocity, and D is the particle diffusion coefficient). Growth, convection, and diffusion represent continuous changes in the number density function, and cannot change the total number of particles alone. On the righthand side, the function $h(v,\boldsymbol{r},t)$ represents all the discontinuous changes, also known as birth and death functions, such as agglomeration, breakage, and nucleation events, which can change the total number of particles in the system.

The asterisk superscript in Eq. 1 represents a dimensional quantity. If an average particle size, $\bar{v}$, is calculated, Eq. 1 can be nondimensionalized. While the particular choice of mean particle volume depends upon the application, some of the more popular choices include the arithmetic mean, the geometric mean, and the harmonic mean (see Fan and Zhu, 1998). Defining the kth moment of the particle volume distribution

$$\mu_k = \int_0^\infty v^k f_1(v)\, dv, \quad (2)$$

the arithmetic mean can be described by $\bar{v}_{ar} = \mu_1/\mu_0$. Nondimensional variables can be defined as

$$\begin{aligned} v &= v^*/\bar{v} \\ \tau &= \chi(\bar{v})t^* \\ f_1 &= \bar{v}^2 f_1^* \\ \dot{V} &= \dot{V}^*/\bar{v}\chi(\bar{v}) \\ \nabla_r &= L\nabla_r^* \\ \dot{\boldsymbol{R}} &= \dot{\boldsymbol{R}}^*/\chi(\bar{v})L \\ D &= D^*/L^2\chi(\bar{v}) \\ h &= h^*\bar{v}^2/\chi(\bar{v}), \end{aligned} \quad (3)$$

where L is an appropriate large-scale length (such as the radius of a pipe), and the time is nondimensionalized by the appropriate function in the birth and death terms. For example, the breakage rate is used in pure breakage equations: $\tau = b(\bar{v})t^*$, which defines the function $\chi(\bar{v})$ in Eq. 3b. In this way the righthand side birth and death functions are also nondimensionalized. The definition for each dimensionless time will be given for each problem studied below.

Equation 2 can now be written as before, but recognized as nondimensional:

$$\frac{\partial}{\partial \tau} f_1 + \frac{\partial}{\partial v} \dot{V} f_1 + \nabla_r \cdot \dot{\boldsymbol{R}} f_1 - \nabla_r \cdot D \nabla_r f_1 = h. \quad (4)$$

It is this form of the equation that will be studied from here on, and for which all results will be displayed.

Two main choices exist for solution of population balance equations: continuous variables or discrete variables. Using continuous variables allows an exact functional form for the number density to be calculated. In particular, given a continuous number density, any derived quantity can be calculated directly and without any additional error than inherent with the number density. If the total amount, Φ, of a particular extensive property ϕ associated with the particles in the

domain is needed, it is given by

$$\Phi(t) = \int_{\Omega_r}\int_{\Omega_x} \phi(\boldsymbol{x},\boldsymbol{r}) f_1(\boldsymbol{x},\boldsymbol{r},t)\, dV_x\, dV_r. \qquad (5)$$

Moment methods are the most common technique for obtaining continuous distributions. Differential equations for the moments, as defined by Eq. 2, are generated by multiplying the population-balance equation (Eq. 4) by v^k and integrating over all v. If the equation for the kth moment can be entirely in terms of moments of degree k or less, the set of moments equations are said to be closed. Closed sets of equations for the moments are the exception rather than the rule, as most agglomeration and breakage kernels generate complicated moment equations.

In addition to the requirement that the moment equations be closed, the moments must be sufficient to describe the particle-size distribution. That is, information about the moments should be sufficient in order to recreate the volume distribution; knowledge of a (finite) number of moments is equivalent to knowledge of the adjustable parameters of an assumed distribution function. In the general case, Shohat and Tamarkin (1943) showed that an infinite number of moments are necessary to completely distinguish a unique distribution. Whitby and McMurry (1997) demonstrate how three moments are sufficient for the log-normal distribution: knowledge of any three integer moments is equivalent to knowledge of the total number of particles, N_0, the geometric mean, v_g, and the standard deviation σ in this case

$$f_{LN}(v)\, dv = \frac{N_0}{v\sigma\sqrt{2\pi}} \exp\left(-\frac{1}{2}\left(\frac{\ln v/v_g}{\sigma} \right)^2 \right) dv \qquad (6)$$

The same can be said for each of the other aforementioned distributions: the modified gamma, Rosin-Rammler, and Weibull distributions.

However, it should be noted that the moments themselves give no information about the type of distribution that is applicable. That is, the exact same three moments can be used equivalently in both the log-normal and modified gamma distributions to generate two distinct particle number density functions. McGraw et al. (1998) contrived an example that emphasizes some of the weaknesses of moment methods. They showed that by multiplying the log-normal distribution by an arbitrary odd function, the resulting function has identical zeroth, first, and second moments as the original log-normal function

$$g(v) = f_{LN}(v)\left[1 + \sin\left(\frac{2\pi \ln(v/v_g)}{\sigma^2} \right) \right]. \qquad (7)$$

Both $g(v)$ and $f_{LN}(v)$ have equal lower-order moments, yet are very different functions, as shown in Figure 1. A modified gamma distribution with the same low-order moments is also plotted in Figure 1 in order to emphasize the argument that three moments do not guarantee a unique function, and the choice of a standard distribution can be a very restrictive assumption.

In the other main computational method, a discrete distribution representation divides the particle volume variable into intervals. Discrete variables are more common, simply because the data are easier to obtain. Sieve analysis yields discrete data; a particle trapped in a tray is contained in a volume interval. However, it is infeasible to know the distribution inside that interval. Computationally, discrete solutions can be more economic and simple to program. On the other hand, errors from discretizing the domain can lead to incorrect derived properties of the particle. The integral in Eq. 5 becomes a sum over the bins, also leading to greater errors.

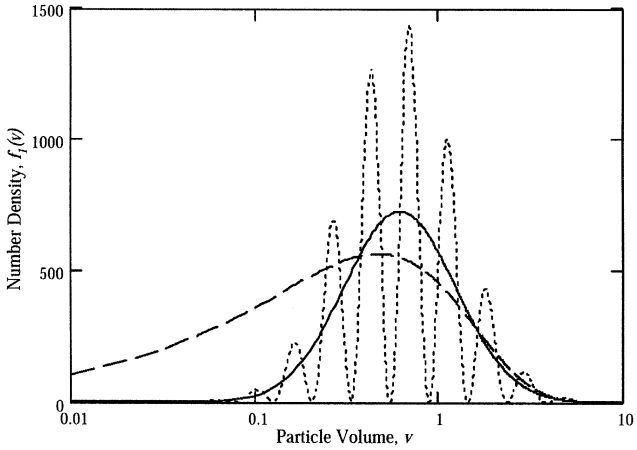

Figure 1. Each of the distributions in the figure have the exact same first three integer moments, μ_0 = 1,000, μ_1 = 1,278, and μ_2 = 2,664; however, the solid line is a log-normal function, the dotted line is the modified log-normal of Eq. 7, and the dashed line is a modified gamma distribution.

Hidy (1965) used a uniform grid, whereas Bleck (1970) was among the first proponents of the geometric grid for pure agglomeration simulations; however, consistency problems with either mass conservation or total numbers became evident, especially for long times. Kumar and Ramkrishna (1996a,b) introduced a discrete technique by which any two moments can be preserved, for example, the zeroth moment corresponding to total number of particles, and the first moment corresponding to total mass, on an arbitrary grid. Particularly advantageous, the arbitrary grid allows for selective refinement to improve the accuracy when rapid changes occur. These and many more discrete simulation techniques are discussed in the review articles by Kostoglou and Karabelas (1994) and Vanni (2000).

Hermite Spectral Method

Consider a change of variables, based upon the log-normal distribution defined in Eq. 6

$$y = \frac{\ln v/v_g}{\sigma} \quad \text{or equivalently} \quad v = v_g \exp(\sigma y) \qquad (8)$$

The log-normal distribution (Eq. 6) can then be written as

$$f_{LN}(v)\, dv = \alpha_0 e^{-(1/2)y^2} dy, \qquad (9)$$

where $\alpha_0 = N_0/\sqrt{2\pi}$. Equation 9 implies the set of Hermite polynomials would be a natural basis set for the solution of population-balance equations via spectral methods. Hermite polynomials are appropriate because they are orthogonal on the interval $(-\infty, +\infty)$ with respect to weight function $\omega(y) = e^{-y^2}$. Several properties of the Hermite polynomials are presented in the Appendix. Natural boundary conditions are also compatible, as the Hermite functions decay to zero at both $y = +\infty$ and $y = -\infty$, which correspond to actual particle volumes of $v = +\infty$ and $v = 0$, at which values the number density function must also be zero.

To use spectral methods, the number density function must also be converted from actual volume, v, to transformed volume, y. Let the number density function of transformed volume be $n(y,\boldsymbol{r},\tau)$. Preserving the number of particles in the distributions from real volume to transformed volume, set

$$n(y)\,dy = f_1(v)\,dv \qquad \text{or} \qquad f_1(v) = n(y)\frac{dy}{dv}. \quad (10)$$

The Jacobian of the transformation, dy/dv, appears, and must be inserted into the population-balance (Eq. 4) with the transformed volume number density

$$\frac{dy}{dv}\left(\frac{\partial n}{\partial \tau} + \frac{\partial \dot{Y} n}{\partial y}\right) + \nabla\cdot\left(\dot{\boldsymbol{R}} n \frac{dy}{dv}\right) - \nabla\cdot\left(D\nabla n \frac{dy}{dv}\right) = h, \quad (11)$$

with the velocity/growth term

$$\dot{Y} = \left(\frac{\partial y}{\partial \tau}\right)_v + \dot{V}\left(\frac{\partial y}{\partial v}\right)_\tau \quad (12)$$

Propose an M-term Hermite function expansion, to be plugged into the population-balance equation (Eq. 11)

$$n(y,\boldsymbol{r},\tau) \approx n_M(y,\boldsymbol{r},\tau) = \sum_{m=0}^{M} \alpha_m(\boldsymbol{r},\tau) e^{-(1/2)y^2} \psi_m(y), \quad (13)$$

where the basis functions, $\psi_m(y)$, are modified (semi-normalized) Hermite functions

$$\psi_m(y) = \frac{H_m(y)}{\sqrt{2^m m!}}, \quad (14)$$

and $H_m(y)$ is the mth Hermite polynomial, defined by (Rodrigues' definition) (Sansone, 1991)

$$H_m(y) = (-1)^m e^{y^2} \frac{d^m}{dy^m} e^{-y^2}, \quad (15)$$

where $H_0(y) = 1$. Equation 9 can now be written as

$$f_{LN}(v)\,dv = \alpha_0 e^{-(1/2)y^2} dy = \alpha_0 \psi_0(y) e^{(-1/2)y^2}\,dy. \quad (16)$$

Clearly, the log-normal distribution is a special case of the proposed Hermite series expansion. Viewed from the opposite perspective, the log-normal distribution is the first term ($m = 0$) in the series; the additional M terms will be employed as corrections to the log-normal approximation, thereby increasing the overall accuracy.

The task at hand is to be able to calculate the spectral coefficients $\{\alpha_m\}$ as they change in time in order to approximate the number density function as the particles experience any dynamic process. Several techniques exist in order to solve for the spectral coefficients; however, they all typically fall into the category of residual methods.

For the population-balance equation (Eq. 11), $Ln - h = 0$, where L is the operator accounting for the lefthand side of the equation, the M-term Hermite approximation is inserted. The result is the residual equation

$$R(y;\alpha_0,\alpha_1,\ldots,\alpha_M) = Ln_M - h \quad (17)$$

The residual is unerringly zero for the exact solution. Choosing the set $\{\alpha_m\}$ that minimizes the residual (Eq. 17) is the task of the form (Eq. 13) of the postulated solution. The method chosen is best known as the pseudospectral method, which is also known as collocation. For this method, the residual is set exactly to zero for a set of carefully chosen points, the collocation points, typically chosen as the zeroes of the $M + 1^{st}$ Hermite polynomial. It is hoped that by setting the residual to zero at several points, the residual will be close to zero almost everywhere (see Boyd, 2001). Specifically, the population-balance equation (Eq. 11) is multiplied by the Dirac delta function, $\delta(y - y_j)$, $j = 0, 1, \ldots, M$, then integrated over all values of y. By the property of the delta function, this simply evaluates the equation at the collocation point, y_j, and the residual equation (Eq. 17) becomes

$$R(y_j;\alpha_0,\alpha_1,\ldots,\alpha_M) = 0; \qquad j = 0,1,\ldots,M. \quad (18)$$

In order to estimate truncation error, all of the presented calculations were run for many different values of M. When the computed solutions did not vary with M, the simulation was considered converged (Boyd, 2001).

Computational Method and Results

Agglomeration

Several population-balance equations will now be solved using the Hermite spectral method and compared with available analytical and other computational results. First, agglomeration events describe the combination of multiple particles into a lesser number of particles. While in highly dense systems, several particles could simultaneously aggregate together, this work is focused solely upon binary events, representative of dilute systems. Agglomeration events can be used to describe several phenomena, including combustion (Brown, 1996), rain formation (Miles et al., 2000), formation of stars (Jorgensen et al., 1995), and polymer chain-length additions (McCoy and Madras, 2001). In binary agglomeration, the righthand side of the population-balance equation (Eq. 4) becomes (Ramkrishna, 2000)

$$h = \frac{1}{2}\int_0^v a(v-\tilde{v},\tilde{v}) f_1(v-\tilde{v}) f_1(\tilde{v})\,d\tilde{v} - f_1(v)\int_0^\infty a(v,\tilde{v}) f_1(\tilde{v})\,d\tilde{v}. \quad (19)$$

The first term is the rate at which particles of volumes $\tilde{v}$ and $v - \tilde{v}$ combine to form a particle of volume v, and the second term is the rate at which the particle of volume v agglomerates with other particles to form larger particles. The agglom-

Table 1. Functions Used in the Collocated Equation

	Function
$T_{jm} =$	$e^{-y_j^2/2}\psi_m(y_j)$
$A_{jm} =$	$e^{-y_j^2/2}\psi_m(y_j)$
$B_{jm} =$	$e^{-y_j^2/2}\psi_m(y_j)y_j$
$C_{jm} =$	$e^{-y_j^2/2}\psi_m(y_j)$
Breakage	
$P_{jm} =$	$\sigma e^{\sigma y_j}\int_{y_j}^{\infty} b(\tilde{y})\nu(\tilde{y})P(y_j\|\tilde{y})e^{-\tilde{y}^2/2}\psi_m(\tilde{y})\,d\tilde{y}$
$Q_{jm} =$	$b(y_j)e^{-y_j^2/2}\psi_m(y_j)$
Agglomeration	
$D_{pjm} =$	$\frac{1}{2}\int_{-\infty}^{y_j} a_0(\theta_j(\tilde{y}),\tilde{y})e^{(\theta_j^2(\tilde{y})/2}\psi_p(\theta_j(\tilde{y}))e^{-\tilde{y}^2/2}\psi_m(\tilde{y})\,d\tilde{y}$
$E_{pjm} =$	$e^{-y_j^2/2}\psi_p(y_j)\int_{-\infty}^{\infty} a_0(y_j,\tilde{y})e^{-\tilde{y}^2/2}\psi_m(\tilde{y})\,d\tilde{y}$
Growth	
$W_{jm} =$	$-e^{(y_j^2/2)\sigma y_j}\left[\dot{V}(y_j)\left(\sqrt{\frac{m}{2}}\,\psi_{m-1}(y_j)-\sigma\psi_m(y_j)\right.\right.$ $\left.\left.-\sqrt{\frac{m+1}{2}}\,\psi_{m+1}(y_j)\right)+\psi_m(y_j)\frac{\partial\dot{V}(y_j)}{\partial y}\right]$

$$\theta_j(\tilde{y}) = \frac{\ln(e^{\sqrt{2}\sigma y_j} - e^{\sqrt{2}\sigma\tilde{y}})}{\sqrt{2}\sigma}.$$

eration frequency, also known as the agglomeration kernel, a, has the dimensions of spatial volume per unit time, and is necessarily reciprocal: $a(u,v) = a(v,u)$.

Considering simply the time-variant population-balance equation, describing the evolution of particles in a batch-vessel, for instance, the population balance written in terms of y variables becomes (after setting convection, diffusion and growth terms to zero)

$$\frac{dy}{dv}\left(\frac{\partial n}{\partial\tau}+\frac{\partial\dot{Y}n}{\partial y}\right) = \frac{1}{2}\int_{-\infty}^{y} a(\theta,\tilde{y})n(\theta)\frac{d\theta}{d\epsilon}n(\tilde{y})\,d\tilde{y} - n(y)\frac{dy}{dv}\int_{-\infty}^{\infty} a(y,\tilde{y})\,d\tilde{y}. \quad (20)$$

Two notes about Eq. 20, θ is the transformed volume of the difference term defined by

$$v - \tilde{v} = v_g(e^{\sigma y} - e^{\sigma\tilde{y}}) = v_g e^{\sigma\theta}. \quad (21)$$

In this way, the number density of actual volume $v - \tilde{v} = \epsilon$ can be transformed into y variables

$$f_1(v-\tilde{v}) = f_1(\epsilon) = n(\theta)\frac{d\theta}{d\epsilon} \quad (22)$$

The lefthand side of Eq. 20 can be evaluated using the chain rule (the second term is zero, as the particle growth rate is assumed to be zero for this pure agglomeration equation)

$$\left(\frac{\partial y}{\partial\tau}\right)_v = \left(\frac{\partial y}{\partial v_g}\right)_v\left(\frac{\partial v_g}{\partial\tau}\right)+\left(\frac{\partial y}{\partial\sigma}\right)_v\left(\frac{\partial\sigma}{\partial\tau}\right) = -\frac{1}{v_g\sigma}\left(\frac{\partial v_g}{\partial\tau}\right)-\frac{y}{\sigma}\left(\frac{\partial\sigma}{\partial\tau}\right). \quad (23)$$

Using the definitions of Eqs. 21–23, then inserting the Hermite approximation of Eq. 13, and finally using the pseudospectral method to generate a residual equation of the form in Eq. 18, the equation for the spectral coefficients becomes, named the collocated equation

Table 2. Functions Used in the Moments Equation

	Function
$K_m(k) =$	$v_g^k\int_{-\infty}^{\infty} e^{\sigma yk}e^{-y^2/2}\psi_m(y)\,dy$
$F(k) =$	$\alpha_m v_g^{k-1}\int_{-\infty}^{\infty} e^{\sigma yk}e^{-y^2/2}\psi_m(y)\,dy$
$G(k) =$	$\alpha_m v_g^k\int_{-\infty}^{\infty} e^{\sigma yk}e^{-y^2/2}\psi_m(y)\left(y+\frac{1}{\sigma}\right)dy$
Breakage	
$U(k) =$	$v_g^k\alpha_m\int_{-\infty}^{\infty} e^{\sigma y(k+1)}\int_{-\infty}^{\infty} b(\tilde{y})v(\tilde{y})P(y\|\tilde{y})e^{-\tilde{y}^2/2}\psi_m(\tilde{y})\,d\tilde{y}\,dy$ $-v_g^k\alpha_m\int_{-\infty}^{\infty} e^{\sigma yk}b(y)e^{-y^2/2}\psi_m(y)\,dy$
Agglomeration	
$L(k) =$	$\frac{1}{2}v_g^k\alpha_m\alpha_p\int_{-\infty}^{\infty}\int_{-\infty}^{\infty} a_0(\theta,\tilde{y})(e^{\sqrt{2}\sigma\theta}+e^{\sqrt{2}\sigma\tilde{y}})^k e^{-\theta^2}\psi_m(\theta)e^{-\tilde{y}^2}\psi(\tilde{y})\,d\tilde{y}\,d\theta$ $-v_g^k\alpha_m\alpha_p\int_{-\infty}^{\infty} e^{\sqrt{2}\sigma yk}e^{-y^2}\psi_m(y)\int_{-\infty}^{\infty} a_0(y,\tilde{y})e^{-\tilde{y}^2}\psi_p(\tilde{y})\,d\tilde{y}\,dy$
Growth	
$Z(k) =$	$-\alpha_m v_g^k\int_{-\infty}^{\infty} e^{\sigma ky}\dot{V}(y)e^{-y^2/2}\left[\sqrt{\frac{m}{2}}\,\psi_{m-1}(y)-\sqrt{\frac{m+1}{2}}\,\psi_{m+1}(y)\right]dy$ $+\alpha_m\frac{v_g^{k-1}}{\sigma}\int_{-\infty}^{\infty} e^{(\sigma k-1)y}\frac{\partial\dot{V}(y)}{\partial y}\psi_m(y)\,dy$

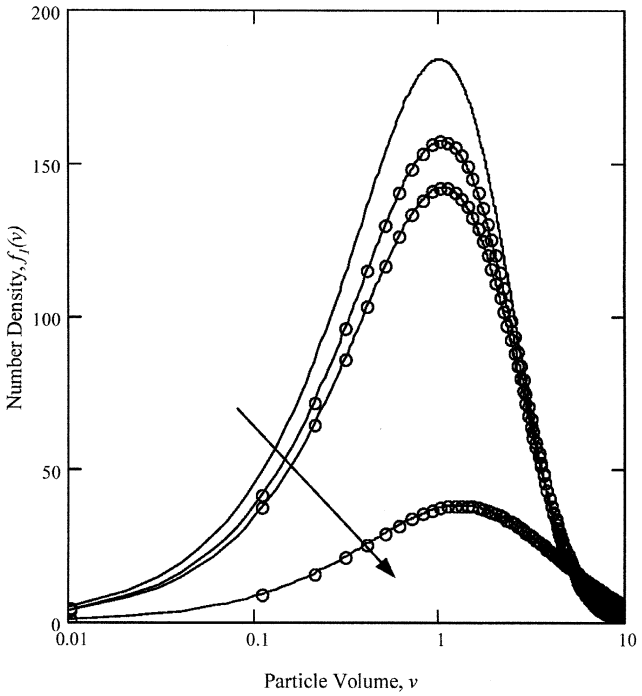

Figure 2. Comparison with constant agglomeration analytical results.

Evolution of the exponential distribution given by Eq. 32, with $N_0 = 250$ and $z = 2$ as it undergoes constant agglomeration with $C = 1.0$. The arrow indicates increasing time, with curves depicted at $\tau = 0.0$, 0.18, 0.3, and 2.66, respectively. Open circles represent analytical results, and the solid curve signifies Hermite spectral method results.

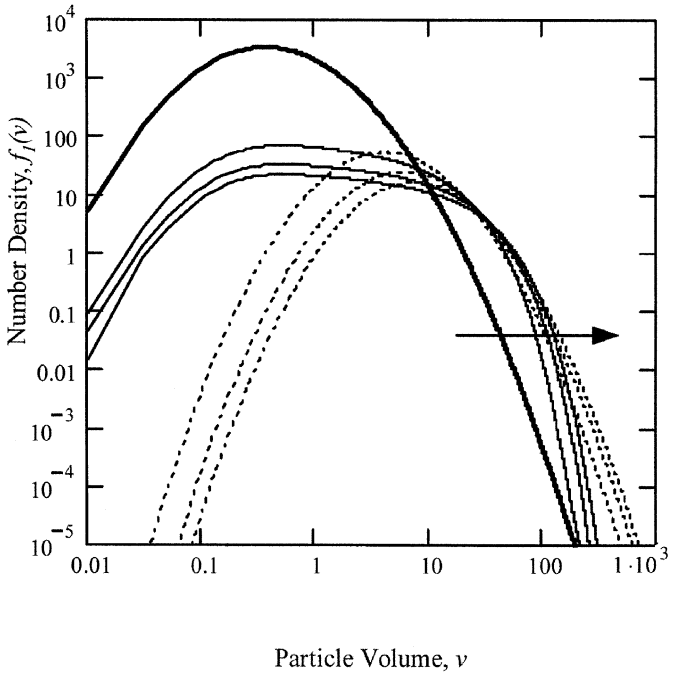

Figure 3. Evolution of the log-normal distribution as it undergoes constant agglomeration with $C = 1.0$.

Curves are depicted at $\tau = 0.0$, 12.9, 19.9, and 24.9, respectively. The thick curve is the initial condition, a log-normal distribution (Eq. 6) with $N_0 = 5{,}000$ and $v_g = \sigma = 1.0$; solid curves depict Hermite spectral and Laplace transform method results; and the dotted curves depict log-normal moments method results.

$$T_{jm}\frac{\partial \alpha_m}{\partial \tau} + A_{jm}\alpha_m \frac{1}{v_g \sigma}\frac{\partial v_g}{\partial \tau} + \left[B_{jm} - C_{jm}\right]\alpha_m \frac{1}{\sigma}\frac{\partial \sigma}{\partial \tau} = \alpha_p\left[D_{pjm} - E_{pjm}\right]\alpha_m \quad (24)$$

where the definitions of Table 1 have been introduced for brevity. Also observe that the repeated indices, m and p, indicate an implied sum from 0 to M. Equation 24 corresponds to $M + 1$ unique equations, one for each collocation point, $j = 0,1, \ldots, M$, enumerated from 0 (least) to M (greatest). Also accounted for are changes in the adjustable parameters v_g and σ, which change the definition of y (Eq. 19).

Moment equations are used to close the last two equations for v_g and σ. When written in y variables, the equation for the rate of change of any moment, k, is

$$\frac{\partial \mu_k}{\partial \tau} = F(k)\frac{\partial v_g}{\partial \tau} + G(k)\frac{\partial \sigma}{\partial \tau} + L(k), \quad (25)$$

with the definitions of Table 2 applied. The righthand side, in general, is indeterminable, and the chain rule may be used to close the set of equations.

$$\frac{\partial \mu_k}{\partial \tau} = \frac{\partial \mu_k}{\partial v_g}\frac{\partial v_g}{\partial \tau} + \frac{\partial \mu_k}{\partial \sigma}\frac{\partial \sigma}{\partial \tau} + \frac{\partial \mu_k}{\partial \alpha_i}\frac{\partial \alpha_i}{\partial \tau} = I(k)\frac{\partial v_g}{\partial \tau} + J(k)\frac{\partial \sigma}{\partial \tau} + K_i(k)\frac{\partial \alpha_i}{\partial \tau}. \quad (26)$$

Combining Eqs. 25 and 26, and named the moments equation

$$(I(k) - F(k))\frac{\partial v_g}{\partial \tau} + (J(k) - G(k))\frac{\partial \sigma}{\partial \tau} + K_i(k)\frac{\partial \alpha_i}{\partial \tau} = L(k). \quad (27)$$

Any value of k other than 0 can be chosen, though 1 and 2 are the most common. In particular, choosing $k = 1$ makes Eq. 27 a conservation of mass. Equation 24 with Eq. 27 embodies the complete set of equations to be solved. While nonlinear in the spectral coefficients, the system is linear in the time derivatives of the dependent variables. A vector of time derivatives can be constructed

$$\boldsymbol{\kappa} = \left[\frac{\partial v_g}{\partial \tau}\ \frac{\partial \sigma}{\partial \tau}\ \frac{\partial \alpha_0}{\partial \tau}\ \frac{\partial \alpha_1}{\partial \tau} \cdots \frac{\partial \alpha_M}{\partial \tau}\right]^T, \quad (28)$$

as the solution to the matrix equation

$$\boldsymbol{R}\boldsymbol{\kappa} = \boldsymbol{f}, \quad (29)$$

with the matrix $\boldsymbol{R}$ defined as

$$\boldsymbol{R} = \begin{bmatrix} I(1)-F(1) & J(1)-G(1) & K_0(1) & K_1(1) & \cdots & K_M(1) \\ I(2)-F(2) & J(2)-G(2) & K_0(2) & K_1(2) & \cdots & K_M(2) \\ \dfrac{A_{0m}\alpha_m}{v_g\sigma} & \dfrac{[B_{0m}-C_{0m}]\alpha_m}{\sigma} & T_{00} & T_{01} & \cdots & T_{0M} \\ \dfrac{A_{1m}\alpha_m}{v_g\sigma} & \dfrac{[B_{1m}-C_{1m}]\alpha_m}{\sigma} & T_{10} & T_{11} & \cdots & T_{1M} \\ \vdots & \vdots & \vdots & \vdots & \vdots & \vdots \\ \dfrac{A_{Mm}\alpha_m}{v_g\sigma} & \dfrac{[B_{Mm}-C_{Mm}]\alpha_m}{\sigma} & T_{M0} & T_{M1} & \cdots & T_{MM} \end{bmatrix} \tag{30}$$

and the forcing function vector

$$\boldsymbol{f} = \left[L(1)\ L(2)\ \alpha_p\left[D_{p0m}-E_{p0m}\right]\alpha_m\ \alpha_p\left[D_{p1m}-E_{p1m}\right]\alpha_m \cdots\ \alpha_p\left[D_{pMm}-E_{pMm}\right]\alpha_m \right]^T \tag{31}$$

A fourth-order Runge-Kutta method is used to propagate the numerical solutions through discretized time.

Several agglomeration problems have analytical solutions available. Through the method of Laplace transforms, the number distribution of particles experiencing constant agglomeration can be solved for at any time (Ramkrishna, 2000). Analytic solutions for the sum and product agglomeration kernels, on the other hand, are only available for certain initial conditions. Scott (1968) also employed the method of Laplace transforms, but was limited to exponential initial conditions to achieve exact solutions. Specifically, Scott's initial distributions were of the form

$$f_1(v,0) = N_0\left(\frac{v}{z}\right)e^{-v/z}, \tag{32}$$

where N_0 and z are adjustable parameters. Note that the initial total number of particles is equal to $N_0 z$.

The constant agglomeration kernel, $a(v,\tilde{v}) = C$, describes a system where every particle truly has an equal chance to agglomerate with any other. It is also able to mimic the Brownian diffusion kernel (Smoluchowski, 1917) for very short times for monodisperse initial conditions; however, its use is typically implemented because of the availability of analytical solutions. The agglomeration kernel itself defines the appropriate dimensionless time, $\tau(t^*) = C\mu_0(0)t^*$. A comparison with the analytical solution of Scott (1968) and the Hermite spectral numerical solution is presented in Figure 2. Numerically, the results are excellent, with less than 1% relative error over the entire curve at the last time presented. Relative error is defined as

$$\%\text{rel.err.} = \frac{\sqrt{\int_0^\infty \left(f_{1,\text{analytic}}(v,\tau) - f_{1\text{Hermite}}(v,\tau)\right)^2 dv}}{\mu_0(\tau)} \tag{33}$$

As expected, for the relatively simple case of constant agglomeration, the Hermite spectral method performs well. Because an exact solution can be achieved for any initial distribution experiencing constant agglomeration, a comparison of the Hermite spectral method and the log-normal method can now be made. Figure 3 is a graphical representation of how an initially log-normal distribution evolves while constant agglomeration occurs. In even this simplest of cases, it is plain to see the inadequacies of the log-normal method. Following the log-normal moments method, the distribution geometric mean increases rapidly, while the standard deviation decreases, resulting in a skinnier distribution moving to the right. On the other hand, the validated Hermite spectral method predicts an ever flatter curve. The log-normal method is able to predict the agglomeration front to a reasonable extent, though the largest particle in the system is erroneous. Where the log-normal curves are the weakest are the lefthand side of the graph—the numbers of small mass particles. In addition, the higher-order moments, as predicted by the log-normal methods, are increasingly inaccurate. Numbers and mass are equal (zeroth and first moments, respectively), but the log-normal second moment is overpredicted by 23% by the last curve. Even worse, the third moment is overpredicted by 76% at the same time.

As was stated earlier, the Hermite series approximation truncated at one term is equivalent to the log-normal distributions. Taken from another point of view, the log-normal distribution is the first-order approximation to the Hermite spectral series. By dimensionless time 24.9, the last curve depicted in Figure 3, the higher-order terms in the series become important. In fact, the first 25 coefficients of the spectral series are nontrivial in describing the fourth curve. The more Hermite spectral terms needed to describe a distribution, the greater that distribution's deviation from log-normality.

Sum agglomeration, $a(v,\tilde{v}) = C(v+\tilde{v})$, can be used as a short-term estimation of shear kernels, often employed in laminar flow situations. Figure 4 displays the comparison between Scott's (1968) analytical results and the Hermite spectral approximation for sum agglomeration. The dimensionless time for product agglomeration is $\tau(t^*) = C\mu_1(0)t^*$. Accuracy is again excellent with the analytical results—less than 2%

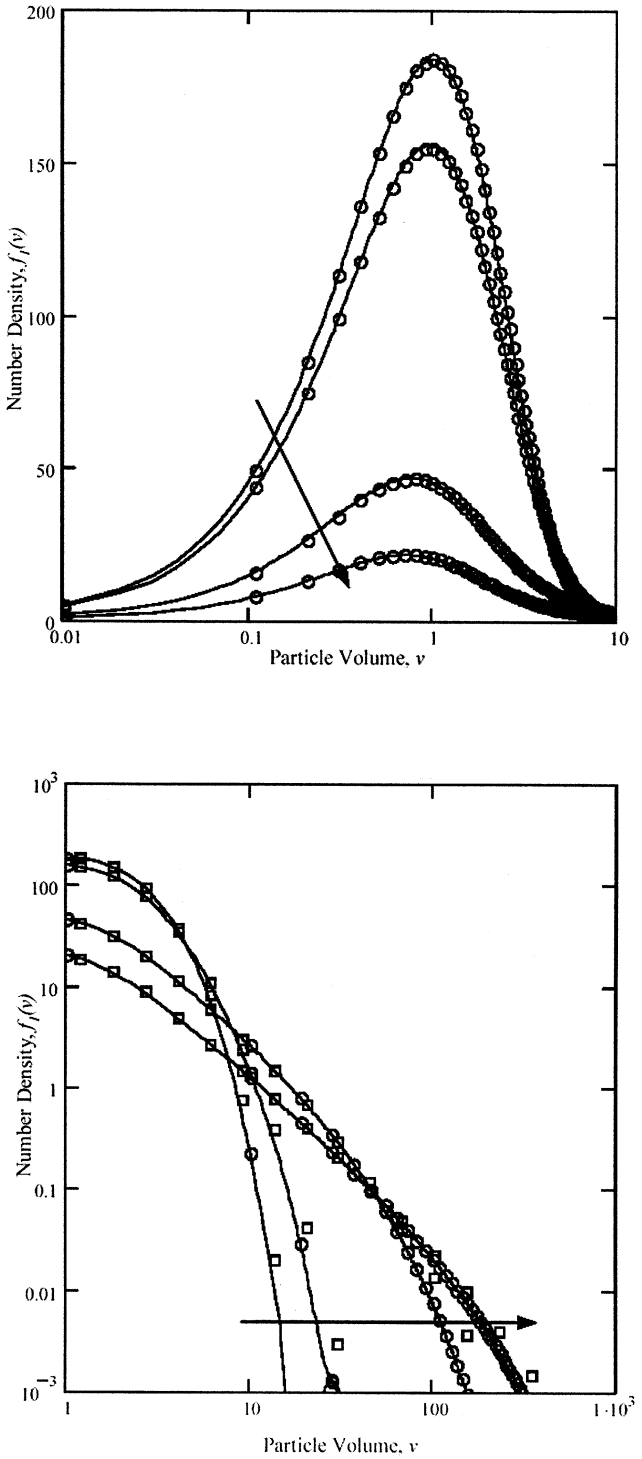

Figure 4. Comparison with sum agglomeration analytical results.

Evolution of the exponential distribution given by Eq. 32, with $N_0 = 250$ and $z = 2$ as it undergoes sum agglomeration with $C = 1.0$. The arrow indicates increasing time, with curves depicted at $\tau = 0.0$, 0.12, 1.15, and 2.0, respectively. Open circles represent analytical results, and the solid curve signifies Hermite spectral method results. The bottom panel is a close-up to show improved accuracy. The axes have been changed to log-log in order to better demonstrate the errors. In addition, the open boxes show results from a Kumar-Ramkrishna discrete method using a geometric grid.

relative error. The improvement in accuracy can be most easily seen in the bottom frame of Figure 4, where the Kumar-Ramkrishna discrete method was also implemented. As reported, when the discrete grid is sparse, an overprediction of the agglomeration front is common (Kumar and Ramkrishna, 1996a). But, the Hermite spectral method captures this front well, at the cost of greater computer time, of course.

The error associated with the Kumar-Ramkrishna discrete method does not appear great until the derived properties of the distributions are examined. Figure 5 displays the prediction of the second moment of the distribution by both the Kumar-Ramkrishna discrete method and the Hermite spectral method. Not surprisingly, the Hermite spectral method has dramatically less error, at the expense of greater computational cost. By the dimensionless time of 2, the Kumar-Ramkrishna discrete method overpredicts the second moment by 75%, whereas the Hermite spectral method shows less than 2% relative error. To be fair, this Kumar-Ramkrishna simulation is only designed to conserve two moments, particle numbers and mass (zeroth and first moments), and makes no guarantee about the second or higher moments. By only accurately predicting two moments, a unique distribution is not guaranteed, as in Figure 1. A main feature of the Hermite spectral method, its ability to interpolate the solution between points with a high-order polynomial, is the primary reason for the greater accuracy of the particle number distribution and all its derived properties.

Product agglomeration, $a(v,\tilde{v}) = Cv\tilde{v}$, is a gelling kernel that also allows for some analytical results. The appropriate definition of the dimensionless time is $\tau(t^*) = C\mu_1^2(0)t^*/\mu_0(0)$. At a dimensionless time of 2, the gelling transition occurs, a mathematical discontinuity where the second moment goes to infinity. Figure 6 displays the comparison between the analytical results and the Hermite spectral numerical results. Excellent agreement is again achieved, with less than a 2% relative error for all results.

Once again the overpredictions by the Kumar-Ramkrishna discrete method do not appear striking until the derived properties of the number density are examined. The second moment as the distribution experiences product agglomera-

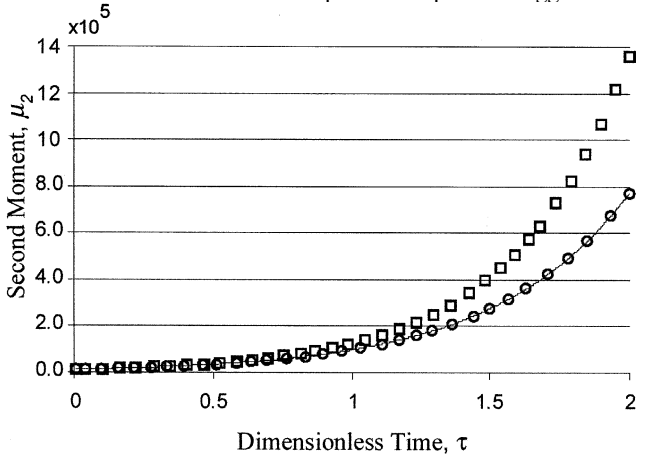

Figure 5. Predictions of the second moment for sum agglomeration by the Kumar-Ramkrishna method (open boxes) and the Hermite spectral method (solid line) as compared with the analytic results (open circles).

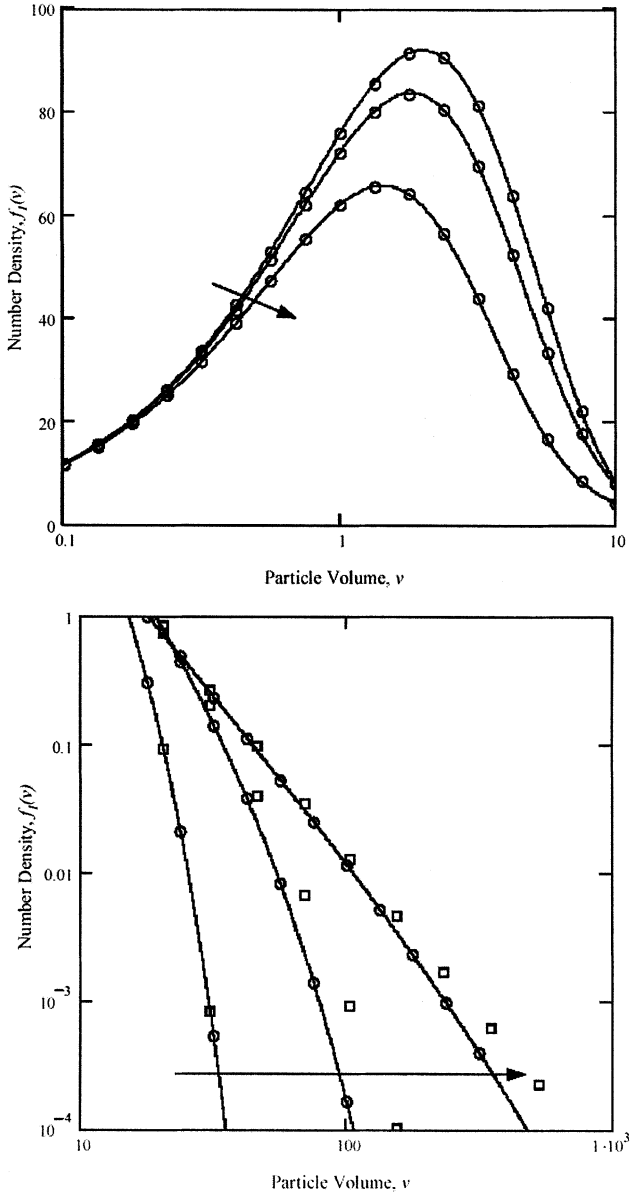

Figure 6. Comparison with product agglomeration analytical results.

Evolution of the exponential distribution given by Eq. 32, with $N_0 = 125$ and $z = 4$ as it undergoes product agglomeration with $C = 1.0$. The arrow indicates increasing time, with curves depicted at $\tau = 0.0, 0.20, 0.80$, respectively. Open circles represent analytical results, and the solid curve signifies Hermite spectral method results. The bottom panel is a close-up to show improved accuracy. The axes have been changed to log-log in order to better demonstrate the errors. The arrow again indicates increasing time, with the solid curves being the Hermite approximation, the open circles the analytical result, and the open boxes the Kumar-Ramkrishna discrete method using a geometric grid.

tion is plotted in Figure 7. As with the previous results, the Kumar-Ramkrishna method overpredicts the second moment by nearly 80% by the dimensionless time of 0.5, while the Hermite spectral method displays less than a 2% error. While the accuracy is better for the interpolative Hermite spectral

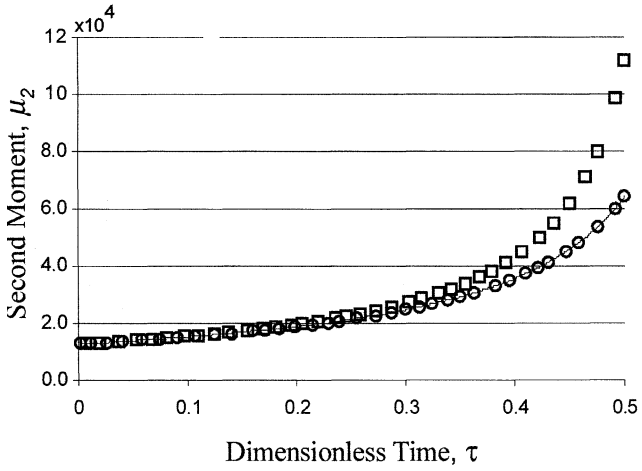

Figure 7. Second moment for product agglomeration.

Predictions of the second moment in product agglomeration by the Kumar-Ramkrishna method (open boxes) and the Hermite spectral method (solid line) as compared with the analytic results (open circles).

method, this accuracy is once more at the expense of greater computational cost.

Growth

Normally, particles do not experience agglomeration solely; growth occurs frequently in combination with agglomeration. Distinctions between condensation and agglomeration typically depend upon the accuracy of the measuring device and/or the application. For example, the addition of one molecule to a "particle" could either be growth or agglomeration. One molecule of water added to a rain droplet is typically seen as an infinitesimal change, that is, growth, whereas the addition of one monomer to a polymer chain can be modeled as agglomeration.

As it is infinitesimal, growth is a convective process on the internal variables. In Eq. 4, the growth rate is given the symbol $\dot{V}$. Models for the growth function vary by process; however, most can be represented by the form $\dot{V}(v) = \dot{G}v^{\gamma}$, where $\dot{G}$ is constant, positive for condensive, and negative for evaporative processes. When the flux to or from the particle is diffusion limited, $\gamma = 1/3$. Whereas, the exponent can be larger for reaction-limited fluxes, $\gamma = 1$ or $\gamma = 2/3$ for volume or surface reactions, respectively. Gelbard and Seinfeld (1979) contain more details. In general, $0 \le \gamma \le 1$.

Pure growth problems, $h = \dot{\boldsymbol{R}} = D = 0$, can be solved via the method of characteristics. In order to validate the Hermite spectral method for growth processes, the same procedure for the agglomeration problem can be carried out, with the exception that both terms in Eq. 12 must be accounted for. The resulting equations can be written as before in matrix form (Eq. 28) with simply a change in the forcing-function vector (again using the definitions of Tables 1 and 2 for brevity)

$$f = \left[Z(1)\, Z(2)\, \frac{W_{0m}\,\alpha_m}{v_g\,\sigma}\ \frac{W_{1m}\,\alpha_m}{v_g\,\sigma} \cdots \frac{W_{Mm}\,\alpha_m}{v_g\,\sigma} \right]^T. \quad (34)$$

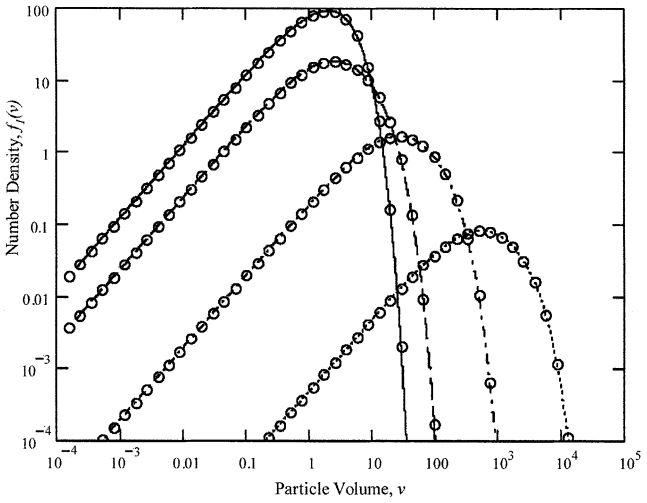

Figure 8. Distributions from linear growth with constant agglomeration.

Evolution of exponential distribution given by Eq. 32, with $N_0 = 125$ and $z = 4$ as it undergoes linear growth and constant agglomeration. The solid line represents the initial condition, whereas the broken lines represent different values of the growth to agglomeration ratio at the dimensionless time $\tau = 3.0$. Specifically, the dashed, the dash-dotted, and the dotted curve correspond to $\Theta = 0.2$, 1.0, 2.0, respectively. The open circles represent analytical results, and the continuous curves signify Hermite spectral method results.

Pure growth problems for both constant and linear growth pose no considerable problems, requiring relatively few spectral basis functions. Relative errors less than 0.1% can often be achieved with $M \leq 10$ (Hamilton, 2002).

One of the advantages of the Hermite spectral method can be demonstrated by solving the population balance with both growth and agglomeration occurring. No extra changes need to be made to the method as outlined earlier; simply, both processes need to be accounted for by summing the respective forcing functions. That is, the righthand side of the collocated equation for simultaneous growth and agglomeration contains the D, E, and W terms from Table 1. The righthand side of the moments equation for simultaneous growth and agglomeration contain the L and Z terms of Table 2. This is in opposition to many discrete simulations where growth doubles the number of equations that need to be solved. Not only do the number of particles in each bin change, but the pivot points of each bin evolve with time (Kumar and Ramkrishna, 1996b).

Ramabhadran et al. (1976) extend the work of Scott (1968) to account for linear growth occurring concurrently with various agglomeration kernels. The ratio between the growth rate and agglomeration rate, Θ, becomes important in determining which dynamic process is dominant. Figure 8 compares the analytic results of Ramabhadran et al. with the Hermite spectral method for linear growth, $\dot{V}(v) = \dot{G}v$, combined with constant agglomeration, $a(v,\tilde{v}) = C$. For this case, the dimensionless ratio is defined as $\Theta = \dot{G}/C\mu_1(0)$. Errors for the simulation are comparable to the errors in the pure agglomeration cases, less than 2% for all growth to agglomeration ratios. For small growth rates, the constant agglomeration effect of flattening the number density curve can be seen. On the other hand, for small agglomeration rates, the shape-preservation and slight dilation typical of linear growth is prevalent.

Breakage

Breakage can be seen as the reverse process of agglomeration. As a single particle breaks, multiple smaller particles are formed. Unlike the agglomeration problem, the usual birth and death functions are typically linear in particle number density. However, similar to the agglomeration problem, this assumption is restricted to less dense systems. In a grinding process, for example, the breakage primarily occurs as the particles contact, and a nonlinear birth and death functional must be used. Also in contrast to the agglomeration problem, greater than binary breakage can be accommodated by the linear breakage functions.

While clearly applicable to particle processes such as communition, the breakage problem is also pertinent in many other situations. Examples include biological systems, specifically, cell division (Mantzaris et al., 2001); astronomy, the size distribution of asteroids after collisions (Piotrowsky, 1953); the car parking problem (Krapivsky, 1992); and food sciences ranging from the grinding of corn and wheat while forming flour (Campbell and Webb, 2001) to the size distribution of chewed food during mastication (Baragar et al., 1996).

The righthand side of population-balance equations describing breakage is written as (Ramkrishna, 2000)

$$h = \int_v^\infty b(\tilde{v})\nu(\tilde{v})P(v|\tilde{v})f_1(\tilde{v})\,d\tilde{v} - b(v)f_1(v), \quad (35)$$

where $b(v)$ is the rate of breakage of particles, v; $\nu(v)$ is the average number of daughter particles formed per breakage event; and $P(v|\tilde{v})$ is the distribution of daughter particles when a particle $\tilde{v}$ breaks. Valid daughter particle distributions must conserve mass and be normalized. Ramkrishna (2000) discusses these conditions in greater detail.

Following the same procedure outlined for the agglomeration and growth problems given earlier, the forcing function for the Hermite spectral method of pure breakage is given by

$$f = \left[U(1)\ U(2)\ \left[P_{0m} - Q_{0m}\right]\alpha_m \left[P_{1m} - Q_{1m}\right]\alpha_m \cdots \left[P_{Mm} - Q_{Mm}\right]\alpha_m\right]^T \quad (36)$$

Once again, the definitions of Tables 1 and 2 have been used for conciseness.

The Hermite spectral method may be used to solve both steady-state limited-breakage and transient-breakage problems. Limited-breakage problems are the solution of the population-balance equation:

$$\frac{\partial f_1(v)}{\partial \tau} = \int_{\max(v,v_m)}^\infty b(\tilde{v})\nu(\tilde{v})P(v|\tilde{v})f_1(\tilde{v})\,d\tilde{v} - b(v)f_1(v)\cup(v - v_m), \quad (37)$$

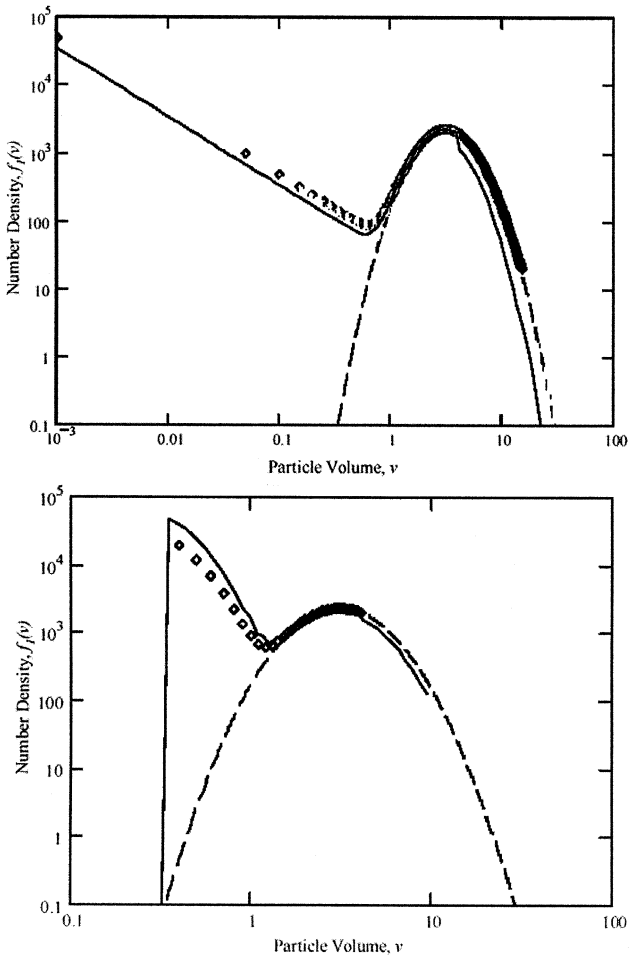

Figure 9. Steady-state distributions from limited breakage.

The static steady states achieved from an initially log-normal distribution, $v_g = 4.0$, $\sigma = 0.5$, and $N_0 = 10{,}000$, plotted as the dashed lines. In the top panel, the daughter particle distribution was given by the power-law breakage kernel with $\eta = -1.0$, and the maximum stable size $v_m = 15.0$. Open diamonds represent the analytical solution, and the solid line is the Hermite spectral method. In the bottom panel, the daughter particle distribution was given by the equal-size breakage kernel with $\eta = 12.0$, and the maximum stable size $v_m = 4.0$. Again, open diamonds represent the analytical solution, and the solid line is the Hermite spectral method.

where $\cup(x)$ is the Heaviside step function. The max function (the lower limit of the integral) and the Heaviside step function are used to ensure only particles with volume greater than v_m undergo breakage. As an example, consider droplets in a stirred tank being broken by the impeller blade. The value of the maximum stable particle/droplet size, v_m, depends upon physical properties and flow conditions (Arai et al., 1977). In the case of pure breakage events, a steady-state solution when all particles are smaller than v_m will eventually be reached. Therefore breakage rate is unimportant, as all particles larger than the maximum stable size will break, given enough time. Kostoglou et al. (1997) describe several analytical results for static steady states from limited breakage problems.

The power kernel, $\nu(\tilde{v})P(v|\tilde{v}) = (\eta+2)v^{\eta}/\tilde{v}^{\eta+1}$, is a simplification of the more generic power law often used to fit

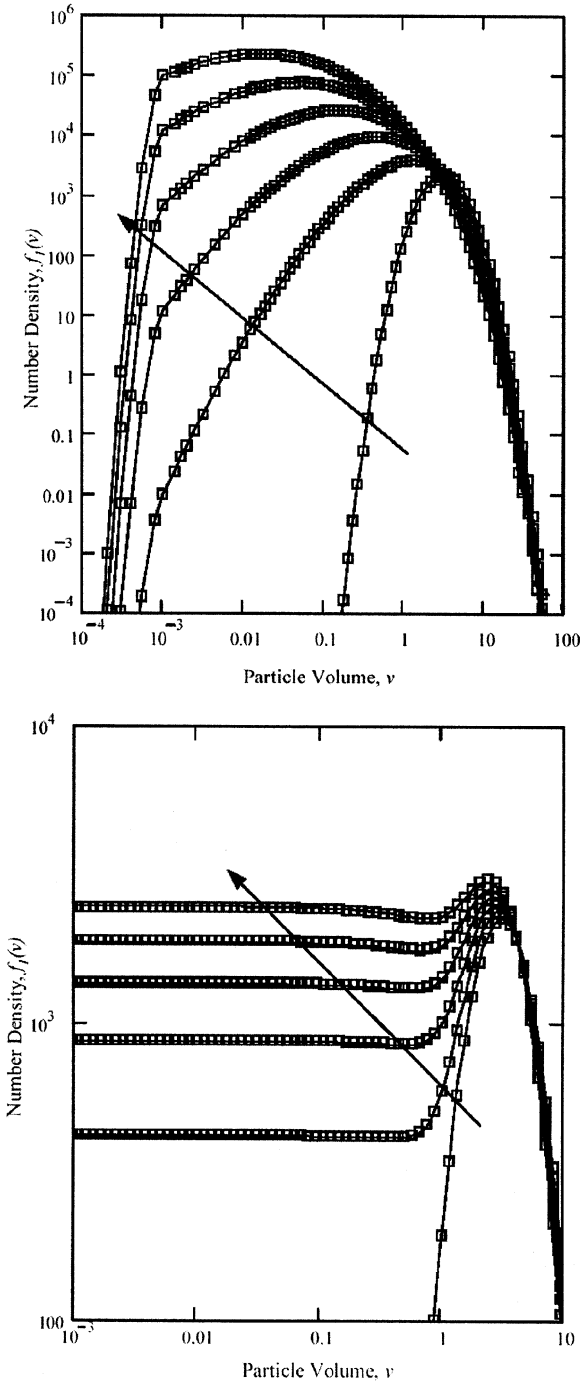

Figure 10. Distributions from transient breakage.

The number distributions from an initially log-normal distribution, $v_g = 4.0$, $\sigma = 0.5$, and $N_0 = 10{,}000$ as it experiences transient breakage. In the top graph, the daughter particle distribution is given by the equal-size breakage kernel with $\eta = 2.0$. The plots are represented at dimensionless time $\tau = 0.0$, 0.4, 0.8, 1.2, 1.6, 2.0, and the arrow indicates increasing time. Breakage rate is given by $b(v) = 200.0$. Open boxes represent the Kumar-Ramkrishna discrete solution data and the solid line is the Hermite spectral method. On the bottom graph, the daughter particle distribution is given by the uniform breakage kernel. The plots are represented at dimensionless time $\tau = 0.0$, 0.009, 0.018, 0.027, 0.036, and the arrow indicates increasing time. Breakage rate is given by $b(v) = v$. Again, open boxes represent the Kumar-Ramkrishna discrete solution data, and the solid line is the Hermite spectral method.

grinding data from quartz, limestone, and cement clinker (Austin et al., 1976) to various wheats when producing flour (Campbell et al., 2001). Figure 9 (top) shows results for a steady-state distribution using the power-law daughter distribution. The Hermite spectral method has reasonable success at capturing the steady state. Problems arise at the endpoints, which are expected, given the pathology of the analytical solution. Sharp discontinuities, like the break at the maximum stable size, are very difficult, practically impossible, to capture with a finite number of terms in a spectral series. Apart from these difficulties, several details of the distribution are handled well. The turning point near $v = 0.7$ is predicted correctly, as well as conservation of mass.

When daughter particles are exactly one ηth the size of the parent particle after breakage, the equal-size kernel is used $\nu(\tilde{v})P(v|\tilde{v}) = \eta\delta(v - \tilde{v}/\eta)$. The bottom panel of Figure 9 shows results for a steady-state distribution resulting from equal-size breakage. Again, the pathology of the function is ill-suited for the Hermite series approximation. Discontinuities exist at both endpoints, $v = 0.33$ and $v = v_m = 4.0$. Yet, the spectral method is able to describe the steady state with less than 10% relative error.

Transient breakage problems may also be solved via the Hermite spectral method. For these problems, breakage rate is now an important function that can also affect the resulting distributions. Most studied breakage rates are written as $b(v) = Bv^{\lambda}$. The breakage rate is also used to define the dimensionless time $\tau = b(\bar{v}_{ar})t^*$.

The method of Kumar and Ramkrishna (1996a) has been validated for equal-size breakage when a sufficient number of discrete bins were used. For comparison, the Hermite spectral method and the Kumar-Ramkrishna method are both used to solve equal-size transient breakage. Figure 10 (top) shows that the agreement between the two computational methods is excellent, less than 0.5% relative disagreement.

Where the equal-size kernel is the limit of a Gaussian daughter-particle probability distribution with zero variance, the uniform distribution $\nu(\tilde{v})P(v|\tilde{v}) = 2/\tilde{v}$ is the limit when the variance goes to infinity. In this case, the probability to create any size daughter particle is equal. Similar to the equal-size kernel, the uniform kernel is more often used in mathematical analysis than for process development. The bottom panel of Figure 10 displays the comparison between the Hermite spectral method and the Kumar-Ramkrishna discrete method. There is an approximately 3% error in the Hermite predictions of the small-volume plateau, attributable again to the pathology of the function. The plateau extends all the way to $v = 0$, yet the Hermite method forces a decay in the function to zero, as particle volume tends to zero.

The sum kernel, $\nu(\tilde{v})P(v|\tilde{v}) = ((m+1)/\tilde{v})[(v/\tilde{v})^m + (1 - v/\tilde{v})^m]$, is a generic U-shaped kernel. It ranges from the uniform kernel at $m = 1$ to increasingly "erosive" as m increases. For larger m, the kernel tends to represent more erosive behavior—preference for widely varying daughter particles. Multimode distributions from unimodal initial conditions are typically very quickly formed from erosion kernels, and the ability of the Hermite spectral method to capture these multimode distributions is an important attribute.

It can be shown that upon using the sum kernel with parameter m, m modes should appear in sufficient time (Kostoglou and Karabelas, 1997). "Cascade fractional breakage" is the name that this phenomenon has been given. Figure 11 contains results from a simulation that exhibits the featured multimodal behavior. By $\tau = 0.170$, the nine breakage modes, in addition to the initial distribution, can be distinctly resolved. A few are distinct by the intermediary time, but not all. This figure is fundamental in exhibiting the strengths of the Hermite spectral method, bearing the entire continuous multimodal function and thereby all the derived properties of the continuous number distribution. The distributions of Figure 11 would be impossible to capture using the unimodal log-normal or modified-gamma methods presented earlier. Note that as the kernel is homogenous, the particle distribution's self-similarity is preserved, as discussed in Hamilton (2002).

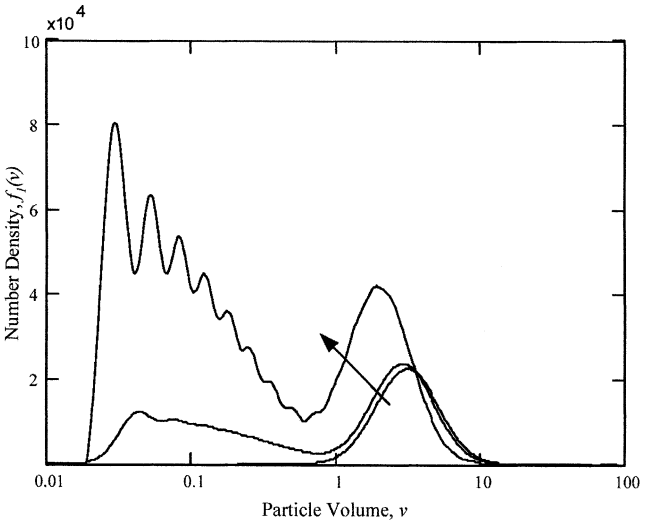

Figure 11. Distributions from transient sum breakage.

The number distributions from an initially log-normal distribution, $v_g = 4.0$, $\sigma = 0.5$, and $N_0 = 10{,}000$ as it experiences sum breakage. Plots are represented at dimensionless time $\tau = 0.0$, 0.086, 0.170 and the arrow indicates increasing time. Daughter particle distribution is given by the sum breakage kernel, with parameter $m = 9$. Breakage rate is given by $b(v) = v$.

A wide variety of problems solved by the Hermite spectral method are validated using both analytical and alternate computational techniques. No significant changes to the method were necessary to solve growth, agglomeration, and breakage problems in both transient and steady-state situations. In the next section, the foundation will be laid to not only solve time-varying problems, but also flow-dominated problems.

Finite-Volume Hermite Spectral Method

The open form of the population balance equation is obtained by integrating Eq. 4 over an arbitrary volume Ω_r (growth and diffusion are assumed zero for simplicity)

$$\frac{\partial}{\partial\tau}\int_{\Omega_r} f_1\, dV_r + \int_{\partial\Omega_{r,\text{in}}} f_1\dot{\boldsymbol{R}}\cdot d\boldsymbol{A}_r + \int_{\partial\Omega_{r,\text{out}}} f_1\dot{\boldsymbol{R}}\cdot d\boldsymbol{A}_r = \int_{\Omega_r} h\, dV_r. \quad (38)$$

Using the divergence theorem, the volume integrals of the convection terms become surface integrals of the fluxes in and out through the boundary of the arbitrary volume. Assuming the particles are very small and follow the motions of the incompressible fluid exactly, the fluid velocity and the particle velocity are equal, $\dot{\boldsymbol{R}} = \boldsymbol{U}_f$, and divergence free. This assumption is rarely justified, but made here to simplify the problem. Lastly, if only steady-state solutions are sought, Eq. 38 becomes

$$\int_{\partial\Omega_{r,\text{in}}} f_1 \boldsymbol{U}_f \cdot d\boldsymbol{A}_r + \int_{\partial\Omega_{r,\text{out}}} f_1 \boldsymbol{U}_f \cdot d\boldsymbol{A}_r = \int_{\Omega_r} h\, dV_r. \quad (39)$$

Equation 39 now represents the generic finite-volume population balance equation.

After converting to y variables, and applying the spectral approximation to the number density function, the 1-D discretized equation can be written as

$$T_{jm}\left[(F\alpha_m)_e - (F\alpha_m)_w\right] - \frac{A_{jm}}{\sigma}\left[\left(F\alpha_m v_g\right)_e - \left(F\alpha_m v_g\right)_w\right]$$

$$-\left(B_{jm} + \frac{C_{jm}}{\sigma}\right)\left[(F\alpha_m\sigma)_e - (F\alpha_m\sigma)_w\right] = h(y)\,\Delta V \quad (40)$$

where F represents the flux across the cell boundary, and the subscripts e and w stand for the values at the east and west interfaces of the cell. ΔV is the volume of the cell. The finite-volume collocated Eq. 40 is easily extendable to 2-D or 3-D problems. An analogous equation can be written for the moments equation.

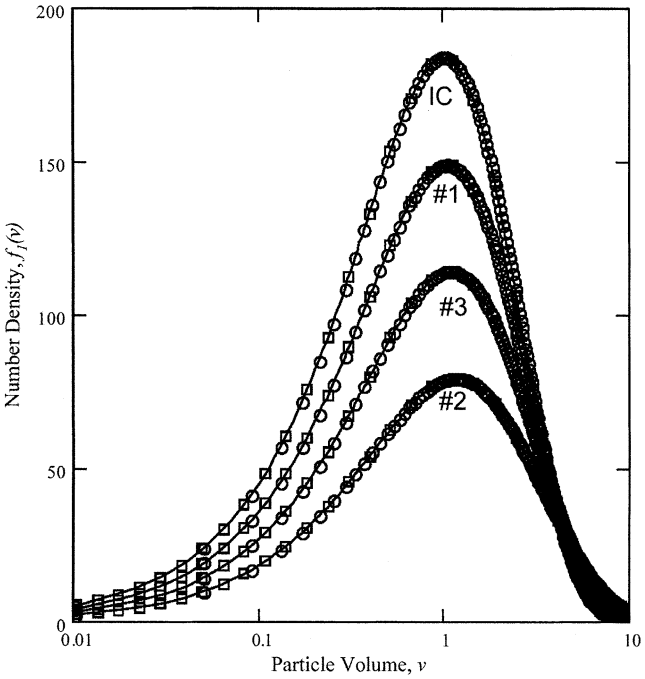

Figure 12. Distributions at the probes from constant agglomeration.

Distributions undergo constant agglomeration with $C = 0.001$. Solid curves represent the Hermite spectral method, boxes represent the Kumar-Ramkrishna discrete technique, and circles represent analytical solutions. The center of cell #1 is at (measured in pipe radii) $(r,z) = (0.25, 1.125)$, #2 is at (0.25, 4.125), and #3 is at (0.85, 4.125).

Table 3. Summary of Results Used to Validate the Hermite Spectral Method

	Analytic Solution	Number of Terms M	Hermite Method Relative Error (%)	Hermite Off-Line + On-Line Time = Total Time (min)	Kumar-Ramkrishna Total Time (min)	Figure(s)
Agglomeration						
Constant	Exponential IC	50	0.9	2+5=7	<1	2,3,12
50-term sum	Exponential IC	50	25*	3+5=8	1	4,5
150-term sum	Exponential IC	150	1.6	89+22=111	1	4,5
50-term product	Exponential IC	50	31*	3+5=8	1	6,7
150-term product	Exponential IC	150	1.8	92+17=109	1	6,7
Breakage						
Power kernel SS	Arbitrary IC	150	13	2+21=23	—	9 top
Equal-size SS	Arbitrary IC	150	9.2	2+16=18	—	9 bot.
Equal-size trans.	N/A	150	0.4	2+9=11	2	10 top
Uniform	N/A	150	3.4	2+9=11	1	10 bot.
Sum	N/A	150	—**	4+25=29	—	11
Growth and Agglomeration						
Constant growth	Arbitrary IC	25	0.04	1+2=3	—	—
Linear growth	Arbitrary IC	25	0.02	1+2=3	—	—
Linear growth and constant agglomeration	Exponential IC	50	1.0	3+5=8	—	8

Note: N/A for Analytic Solution indicates the Hermite spectral method was compared against the Kumar-Ramkrishna discrete method.
*Indicates the onset of instability; using the larger number of terms remedied this error.
**Indicates that since no other method was used on this problem, no error comparison could be made.

This finite-volume methodology for simple flow can be analytically validated for the entrance region to a pipe. The carrier fluid enters the pipe with plug flow at a Reynolds number of 10. Downstream, the fluid takes on the parabolic velocity profile. Because the flow is incompressible, and streamlines do not cross, the method of characteristics may be used to achieve analytic results for simple population-balance problems.

Figure 12 compares the finite-volume Hermite spectral method with analytical results along characteristics for constant agglomeration. The discretization of the domain was 24 equally spaced axial cells and 10 equal-sized radial cells, for a total of 240 control volumes. Agreement is once again exceptional, less than 1% relative error at all three test locations.

Discussion and Conclusions

A new technique for solving population-balance equations has been validated and applied to numerous problems. The Hermite spectral method, based upon adding correction terms to the log-normal method, is applicable to problems involving agglomeration, breakage, and particle growth. Table 3 contains an overview of all the results used to validate the Hermite spectral method, along with the relative accuracy and the time taken for each problem. Both off-line and on-line time is reported to ensure fair comparisons. Off-line time is generally that time that is required to compute the entries in the matrices for each index ranging from 0 to M. For large M ($M > 25$), v_g, and σ are essentially time invariant. Therefore, the definitions of Tables 1 and 2 can be calculated off-line; a database can be stored so that recalculation for different simulations becomes unnecessary. All computations were performed on an 800-MHz Pentium III computer, with 128 MB RAM, to guarantee fair comparisons.

The cost of the greater accuracy the Hermite spectral method provides can now be clearly seen. Hermite spectral calculations can take up to a factor of 25 times longer to arrive at the same simulated time, as compared with the Kumar-Ramkrishna discrete method, assuming the off-line cost is not included. The interpolative ability of the Hermite spectral method does lead to more accurate number density functions, and therefore more accurate predictions of particle properties. Figures 5 and 7 demonstrate this by comparing the predicted second moment by each method. While more costly, the Hermite spectral method is far more precise. Hermite methods are also able to describe multimodal distributions, an impossible task for the original log-normal methods.

Almost any type of population balance problem can be analyzed using the Hermite spectral method. In comparison to other methods, the sacrifice is speed for the benefit of accuracy. Admittedly, the log-normal method is quicker and easier to implement, but cannot capture the true distributions that are generated by population-balance problems. Evidence of this statement can be seen directly from the method, as the first term of the Hermite series is the log-normal function. If the log-normal method were sufficient, only the first spectral coefficient would be necessary, which is clearly not the case. Figure 3 graphically proves this point. Even more striking is the inability of the log-normal method to solve the most simple agglomeration problem, the constant kernel. On the other hand, the Hermite series method is adaptive enough that, until another function is necessary, the coefficient remains zero. The Hermite spectral method builds upon the foundation the log-normal method has laid, and consequently results in a greater level of accuracy.

Acknowledgments

The authors thank NSF/IGERT (fund #DGE-99-72770) and the Dow Chemical Company for their financial support of this work.

Literature Cited

Abramowitz, M., and I. A. Stegun, eds., *Handbook of Mathematical Functions with Formulas, Graphs, and Mathematical Tables*, Dover, New York (1965).

Arai, K., M. Konno, Y. Matunaga, and S. Saito, "Effect of Dispersed-Phase Viscosity on Maximum Stable Drop Size for Breakup in Turbulent Flow," *J. Chem. Eng. Jpn.*, **10**, 325 (1977).

Austin, L., K. Shoji, V. Bhatia, V. Jindal, K. Savage, and R. Klimpel, "Some Results on the Description of Size Reduction as a Rate Process in Various Mills," *Ind. Eng. Chem. Process Des. Dev.*, **15**, 187 (1976).

Baragar, F. A., A. van der Bilt, and H. W. van der Glas, "An Analytic Probability Density for Particle Size in Human Mastication," *J. Theor. Biol.*, **181**, 169 (1996).

Bleck, R., "A Fast, Approximate Method for Integrating the Stochastic Coalescence Equation," *J. Geophys. Res.*, **75**, 5165 (1970).

Boyd, J. P., "Asymptotic Coefficients of Hermite Function Series," *J. Comput. Phys.*, **54**, 382 (1984).

Boyd, J. P., *Chebyshev and Fourier Spectral Methods*, 2nd ed., Dover, New York (2001).

Brown, D. P., "Development of a Three-Dimension Coupled Flow, Species and Aerosol Model: Applications to Particle Deposition in Gas Turbines and Aerosol Formation and Growth in Jet Engine Exhausts," PhD Thesis, Univ. of Cincinnati, Cincinnati, OH (1996).

Brown, W. K., and K. H. Wohletz, "Derivation of the Weibull Distribution Based on Physical Principles and its Connection to the Rosin-Rammler and Lognormal Distributions," *J. Appl. Phys.*, **78**, 2758 (1995).

Campbell, G. M., and C. Webb, "On Prediction Roller Milling Performance Part I: The Breakage Equation," *Powder Technol.*, **115**, 234 (2001).

Devore, J. L., *Probability and Statistics for Engineering and the Sciences*, 4th ed., Duxbury Press, Pacific Grove, CA (1995).

Dunbar, C. A., and A. J. Hickey, "Evaluation of Probability Density Functions to Approximate Particle Size Distributions of Representative Pharmaceutical Aerosols," *J. Aerosol Sci.*, **31**, 813 (2000).

Fan, L.-S., and C. Zhu, *Principles of Gas-Solids Flows*, Cambridge Univ. Press, Cambridge (1998).

Galler, G. M., "Evaluation of the Hermite Polynomial H_N(x) by Recursion," *Collected Algorithms from ACM*, Assoc. Comput. Mach., New York (1980).

Gelbard, F. M., and J. H. Seinfeld, "Exact Solution of the General Dynamic Equation for Aerosol Growth by Condensation," *J. Colloid Interface Sci.*, **68**, 363 (1979).

Greblicki, W., and M. Pawlak, "Hermite Series Estimates of a Probability Density and Its Estimates," *J. Multivar. Anal.*, **15**, 174 (1984).

Hamilton, R. H., "Beyond Log-Normal Distributions; A Hermite Spectral Method for Solving Population Balance Equations of Agglomeration Breakage, Growth, and Simple Particle Flow," MS Thesis, Purdue Univ., West Lafayette, IN (2002).

Hidy, G. M., "On the Theory of the Coagulation of Noninteracting Particles in Brownian Motion," *J. Colloid Interface Sci.*, **20**, 123 (1965).

Jorgensen, H., V. M. Lipunov, I. E. Panchenko, K. A. Postnov, and M. E. Prokhorov, "Cosmological Rates of Coalescing Neutron-Stars and GRB," *Astrophys. Space Sci.*, **231**, 389 (1995).

Kostoglou, M., and A. J. Karabelas, "Evaluation of Zero Order Methods for Simulation Particle Coagulation," *J. Colloid Interface Sci.*, **163**, 420 (1994).

Kostoglou, M., and A. J. Karabelas, "An Explicit Realtionship Between Steady-State Size Distribution and Breakage for Limited Breakage Processes," *J. Phys. A*, **30**, L685 (1997).
Kostoglou, M., S. Dovas, and A. J. Karabelas, "On the Steady State Size Distribution of Dispersions in Breakage Processes," *Chem. Eng. Sci.*, **52**, 1285 (1997).
Krapivsky, P. L., "Kinetics of a Random Sequential Parking on a Line," *J. Stat. Phys.*, **69**, 135 (1992).
Kumar, S., and D. Ramkrishna, "On the Solution of Population Balance Equations by Discretization—I. A Fixed Pivot Technique," *Chem. Eng. Sci.*, **51**, 1311 (1996a).
Kumar, S., and D. Ramkrishna, "On the Solution of Population Balance Equations by Discretization—II. A Moving Pivot Technique," *Chem. Eng. Sci.*, **51**, 1333 (1996b).
Mantzaris, N. V., P. Daoutidis, and F. Srienc, "Numerical Solution of Multi-Variable Cell Population Balance Models: I. Finite Difference Methods," *Comput. Chem. Eng.*, **25**, 1411 (2001).
Markowski, G. R., J. L. Dwons, and J. L. Reese, "Submicrometer Aerosol Size Distributions from an Oil-Fired Boiler," *Aerosols: Science, Technology, and Industrial Applications of Airborne Particles*, B. Y. H. Liu et al., eds., Elsevier Science, New York (1984).
McCoy, B. J., and G. Madras, "Discrete and Continuous Models for Polymerization and Depolymerization," *Chem. Eng. Sci.*, **56**, 2831 (2001).
McGraw, R., S. Nemesure, and S. E. Schwartz, "Properties and Evolution of Aerosol with Size Distributions Having Identical Moments," *J. Aerosol Sci.*, **29**, 761 (1998).
Miles, N. L., J. Verlinde, and E. E. Clothiaux, "Cloud Droplet Size Distributions in Low-Level Stratiform Clouds," *J. Atmos. Sci.*, **75**, 295 (2000).
Montroll, E. W., and M. F. Shlesinger, "On the Wonderful World of Random Walks," *Nonequilibrium Phenomena II From Stochastics to Hydrodynamics*, J. L. Lebowitz and E. W. Montroll, eds., North-Holland Physics Publishing, Amsterdam (1984).
Park, S. H., and K. W. Lee, "Log-Normal Size Distribution Theory for Deposition of Polydisperse Aerosol Particles," *Nucl. Sci. Eng.*, **135**, 288 (2000).
Peterson, T. W., "Similarity Conditions for the Population Balance Equation Describing Particle Fragmentation," *Aerosol Sci. Technol.*, **5**, 93 (1986).
Piotrowsky, P. L., "The Collisions of Asteroids," *Acta Astron.*, **5**, 115 (1953).
Ramabhadran, T. E., T. W. Peterson, and J. H. Seinfeld, "Dynamics of Aerosol Coagulation and Condensation," *AIChE J.*, **22**, 840 (1976).
Ramkrishna, D., *Population Balances: Theory and Application to Particulate Systems in Engineering*, Academic Press, San Diego (2000).
Rosen, J. M., and R. Greegor, "Jet Engine Soot Emission Measured at Altitude," *J. Aircraft*, **11**, 243 (1974).
Sansone, G., *Orthogonal Functions*, Dover, New York (1991).
Scott, W. T., "Analytic Studies of Cloud Droplet Coalescence I," *J. Atmos. Sci.*, **25**, 54 (1968).
Shohat, J. A., and J. D. Tamarkin, *The Problem of Moments*, American Mathematical Society, New York (1943).
Smoluchowski, M., "Versuch einer Mathematischen theori der Koagulationskinetik kollider Losungen," *Zeitschrift fur Physikallsche Chemie-Leipig*, 92, 129 (1917).
Szego, G., *Orthogonal Polynomials*, American Mathematical Society, New York (1981).
Tang, T., "The Hermite Spectral Method for Gaussian-Type Functions," *SIAM J. Sci. Comput.*, **14**, 594 (1993).
Testud, J., S. Oury, R. A. Black, P. Amayenc, and X. K. Dou, "The Concept of a 'Normalized' Distribution to Describe Raindrop Spectra: A Tool for Cloud Physics and Cloud Remote Sensing," *J. Appl. Meteorol.*, **40**, 1118 (2001).
Vanni, M., "Approximate Population Balance Equations for Aggregation-Breakage Processes," *J. Colloid Interface Sci.*, **221**, 143 (2000).
Weideman, J. A. C., "The Eigenvalues of Hermite and Rational Spectral Differentiation Matrices," *Numer. Math.*, **61**, 409 (1992).
Whitby, E. R., and P. H. McMurry, "Modal Aerosol Dynamics Modeling," *Aerosol Sci. Technol.*, **27**, 673 (1997).
Wright, D. L., Jr., "Retrieval of Optical Properties of Atmospheric Aerosols from Moments of the Particle Size Distribution," *J. Aerosol Sci.*, **31**, 1 (2000).

Appendix: Properties of Hermite Polynomials

One of the first works to study a Hermite series in order to estimate a probability density and the accuracy of that approximation is by Greblicki and Pawlak (1984). Using Rodrigues' definition, Eq. 15, the first few Hermite polynomials are

$$H_0(y) = 1$$
$$H_1(y) = 2y$$
$$H_2(y) = 4y^2 - 2$$
$$H_3(y) = 8y^3 - 12y. \qquad \text{(A1)}$$

Coefficients of the first thirteen Hermite polynomials are given by Abramowitz and Stegun (1965), and any Hermite polynomial may be calculated via recursion techniques (Galler, 1980). For example, two recurrence relations are known (Szego, 1981):

$$H_{m+1}(y) + 2yH_m(y) + 2mH_{m-1}(y) = 0 \qquad \text{(A2)}$$

$$\frac{dH_m(y)}{dy} = 2mH_{m-1}(y). \qquad \text{(A3)}$$

As mentioned in the article text, Hermite polynomials are orthogonal on the entire real line with weight, $\omega(y) = e^{-y^2}$

$$\int_{-\infty}^{\infty} H_n(y)H_m(y)e^{-y^2}dy = (H_n, H_m) = 2^m m!\sqrt{\pi}\,\delta_{mn}, \quad \text{(A4)}$$

from which the normalization coefficients are found. It is of crucial importance to use the seminormalized functions of Eq. 14 (the factor of $\pi^{1/4}$ is relatively unimportant) for any number of functions greater than a middling number of M, $M \approx 20$, as computational overflow errors become increasingly common. This can be clearly seen by the asymptotic expansion of $H_m(y)$ (Boyd, 1984):

$$H_m(y) \sim \exp\left(\frac{y^2}{2}\right)\frac{m!}{(0.5m)!}\cos\left(\sqrt{2m+1} - 0.5m\pi\right), \quad \text{(A5)}$$

whereas the expansion as proposed in Eq. 25 is bounded

$$\left|e^{-(1/2)y^2}\psi_m(y)\right| \le 0.816 \qquad \text{(A6)}$$

for all m, and all real y (Boyd, 2001).

Some numerical stability properties of the Hermite spectral method are particularly attractive. For discrete-time marching, a Hermite series approximation is stable up to a discrete-time step of order $O(M^{-1})$, whereas Fourier or Chebyshev approximations are only stable for $O(M^{-2})$ and $O(M^{-4})$, respectively (Weideman, 1992).

Spectral methods on infinite domains exhibit subgeometric convergence, and the Hermite polynomials are no exception (Boyd, 2001). In fact, Hermite polynomials typically converge so leisurely that often a scaling factor is chosen to expedite convergence:

$$u(y) \approx \sum_{m=0}^{M} \alpha_m \psi(\beta y) e^{-(1/2)\beta^2 y^2},$$

which is equivalent to

$$u\left(\frac{y}{\beta}\right) \approx \sum_{m=0}^{M} \alpha_m \psi(y) e^{-(1/2)y^2}. \tag{A7}$$

Tang (1993) offers a method to estimate the scaling factor. Suppose a function has finite support on the interval $[W, -W]$, that is, the function is almost zero outside this interval and does not contribute much to $\{\alpha_m\}$. Let γ_0 represent the maximum zero of the $M+1^{\text{st}}$ Hermite polynomial. Tang estimates the scaling factor with success as

$$\beta = \frac{\gamma_0}{W}. \tag{A8}$$

Explicit convergence rates of the spectral coefficients depend strongly upon the pathology of the function being approximated. When the approximated function decays as e^{-qy^2}, for constant q, supergeometric converge can be observed. However, if the function is simply decaying exponentially, e^{-qy}, or worse, then the general estimate becomes

$$\alpha_m \to O\left(e^{-W\sqrt{2m+1}}\right), \qquad m \gg 1, \tag{A9}$$

where W is the width of compact support, as earlier. By the definitions in Boyd (2001), this Eq. A9 displays subgeometric convergence with index $r = 1/2$. An even worse case may occur when the function only decays algebraically, as the spectral coefficients may decay algebraically as well.

Manuscript received Sept. 4, 2002, and revision received Mar. 4, 2003.